JOURNAL OF COMPUTATIONAL PHYSICS 42, 124–140 (1981)

Transient Eddy Current Analysis on Thin Conductors with Arbitrary Connections and Shapes

AKIHISA KAMEARI

Mitsubishi Atomic Power Industries, Inc., 1-297 Kitabukuro, Omiya, Saitama, Japan

Received August 20, 1980

The numerical method for analyzing transient eddy currents on thin conductors with arbitrary connections and shapes is presented. The eddy currents are described by current functions and discretized in the usual manner of the finite element method. This method is successfully applied to the eddy currents on a sphere surface, a square plate and INTOR-J primary shield. It is shown that this method is accurate and efficient to analyze the eddy currents on complicated conductor structures.

I. INTRODUCTION

In magnetically confined fusion devices like Tokamak, time varying magnetic fields induce transient eddy currents in conductive structures, i.e., vacuum chambers, blankets, shields, supports and others. The eddy currents exert mechanical loading to the structures by the interaction with magnetic fields and the loading must be considered in the structural strength analysis. The error fields by the eddy currents have important effects on the plasma behaviours. And the Joule heat depositions by the eddy currents are not negligible in the superconducting toroidal magnet casings and others.

In this paper, transient eddy currents on thin conductors are analyzed numerically. Various methods have been reported in the analysis of the eddy currents on thin conductors [1–5]. But the methods are applicable only to limited cases or are difficult to apply to more complicated structures. In this paper, the earlier work [1] is generalized and the method presented is the calculation of eddy currents on thin conductors with arbitrary connections and shapes when time varying magnetic fields are applied externally. In this method the eddy currents on thin conductors are described by current functions and energy integrals are represented by means of the current functions. The conductor surface is divided into finite elements and the energy integrals are reduced to discrete forms. The circuit equations of nodal values of current functions are formulated.

In the application of the thin conductor approximation, the skin time of the conductor $\tau_{skin} \simeq \mu_0 \sigma d^2$ (μ_0 is the vacuum permeability, and σ and d are the electric conductivity and the thickness of the conductor, respectively) must be sufficiently small compared with the characteristic time of the external field variations. The

0021-9991/81/070124-17$02.00/0

thickness of the conductor is neglected and the current is assumed to flow in the infinitesimally thin conductor, i.e., on the conductor surface.

In Section II, basic formulations of equations for eddy currents are presented. In Section III, discretization of the conductor surfaces to finite elements is formulated. In Section IV, the numerical method is applied to the eddy currents on a sphere surface, a square plate and INTOR-J primary shield and discussed. In Appendix A, the eddy currents on a sphere surface are formulated analytically.

II. Basic Formulations

A thin conductor structure is divided into subconductors S_n's ($n = 1,..., N_{sub}$), each of which is bounded by a simple closed boundary C_n. Each subconductor is insulated or connected with other subconductors or itself only on its boundary. There is neither source nor sink of current on the interior of each subconductor. The normal unit vector $\mathbf{n}(\mathbf{x})$ at each position $\mathbf{x}$ on the subconductors and the boundary direction of each subconductor are defined as shown in Fig. 1.

The current divergence is equal to zero on each subconductor, so the current linear density is described by a current function V which is a function of time and position on the subconductor [6] and given by

$$\mathbf{j} = \nabla V \times \mathbf{n}. \tag{1}$$

The operations of vector differentiation on a surface are defined in Ref. [6]. The current flows along the lines of $V =$ constant. An arbitrary constant can be added to V, and V can and must be fixed to zero at a certain point on each subconductor to eliminate the arbitrariness.

The magnetic vector potential $\mathbf{A}$ at any position $\mathbf{X}$ induced by the current on the conductor is given by

$$\mathbf{A}(\mathbf{X}) = \frac{\mu_0}{4\pi} \int \frac{\mathbf{j}(\mathbf{x})}{|\mathbf{X} - \mathbf{x}|}\, ds. \tag{2}$$

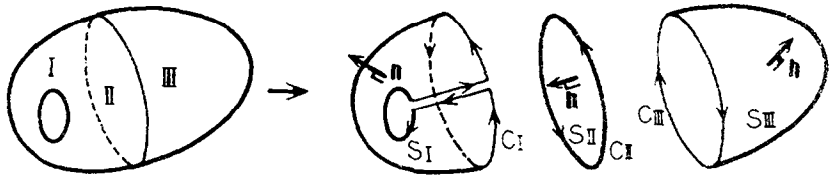

FIG. 1. A connected thin conductor and its division into subconductors.

Here, the integration is all over the conductor surface. And the total magnetic energy by the current on the conductor is given by a double area integration,

$$U_m = \frac{1}{2}\int_s \mathbf{A}\cdot\mathbf{j}\,ds = \frac{\mu_0}{8\pi}\int_s\int_s \frac{\mathbf{j}(\mathbf{x})\cdot\mathbf{j}(\mathbf{x}')}{|\mathbf{x}-\mathbf{x}'|}\,ds\,ds'. \tag{3}$$

When an external magnetic field is represented by magnetic vector potential $\mathbf{A}^{ex}$, the mutual magnetic energy between the current on the conductor and the external magnetic field is given by

$$U_e = \int_s \mathbf{A}^{ex}\cdot\mathbf{j}\,ds. \tag{4}$$

The total Joule loss per unit time by the current on the conductor is given by

$$W_j = \int_s (\rho_{||} j_{||}^2 + \rho_{\perp} j_{\perp}^2)\,ds. \tag{5}$$

Here, $\rho_{||}$ and $\rho_{\perp}$ are the electric area resistivities of the conductor in the principal directions and $j_{||}$ and $j_{\perp}$ are the current density components in the principal directions. The components are given by $j_{||} = \boldsymbol{\tau}_{||}\cdot\mathbf{j}$ and $j_{\perp} = \boldsymbol{\tau}_{\perp}\cdot\mathbf{j}$, where $\boldsymbol{\tau}_{||}$ and $\boldsymbol{\tau}_{\perp}$ are the unit vectors in the principal directions.

Boundary conditions are formulated as follows. Consider a boundary line C on which one or several subconductors are connected as shown in Fig. 2. The total current flowing into C is equal to zero, so the boundary condition is given by

$$\sum_n{}' \pm \frac{\partial V_n}{\partial l} = 0. \tag{6}$$

Here, V_n is the current function on the subconductor S_n, V_n is differentiated along C and the summation is for all subconductor boundaries connected on C with the positive sign when the direction of the differentiation coincides with the direction of C_n or with the negative sign when it is inverse. When only one subconductor boundary is on C, Eq. (6) shows that V is constant along C and current does not intersect C. Equation (6) is a generalization of Kirchhoff's first law.

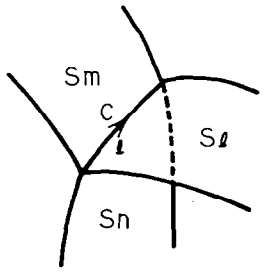

FIG. 2. A boundary line C where three subconductors are connected.

Symmetry conditions are formulated as follows. Now, it is assumed that the conductor is invariant for a certain transformation T (rotation, inversion or reflection). In this case, for any point $\mathbf{x}$ on the conductor, the transformed point $\mathbf{x}'$ given by

$$\mathbf{x}' = T\mathbf{x} \tag{7}$$

is also on the conductor and normal vectors, principal vectors and electric area resistivities have the relations given by

$$\mathbf{n}(\mathbf{x}') = T\mathbf{n}(\mathbf{x}), \qquad \boldsymbol{\tau}_{\parallel}(\mathbf{x}') = T\boldsymbol{\tau}_{\parallel}(\mathbf{x}), \qquad \boldsymbol{\tau}_{\perp}(\mathbf{x}') = T\boldsymbol{\tau}_{\perp}(\mathbf{x}),$$
$$\rho_{\parallel}(\mathbf{x}') = \rho_{\parallel}(\mathbf{x}) \qquad \text{and} \qquad \rho_{\perp}(\mathbf{x}') = \rho_{\perp}(\mathbf{x}). \tag{8}$$

If the current function has a relation given by

$$V(\mathbf{x}') = I\,V(\mathbf{x}), \tag{9}$$

here I is equal to 1 or -1, then the current density has the relation given by

$$\mathbf{j}(\mathbf{x}') = \nabla' V(\mathbf{x}') \times \mathbf{n}(\mathbf{x}') = I \cdot \det T \cdot T\mathbf{j}(\mathbf{x}), \tag{10}$$

and similarly the magnetic vector potential has a relation given by

$$\mathbf{A}(\mathbf{x}') = I \cdot \det T \cdot T\,\mathbf{A}(\mathbf{x}), \tag{11}$$

here the determinant of T is equal to 1 or -1. Inversely, if the external magnetic field $\mathbf{A}^{ex}$ has the relation of Eq. (11), the current fumnction V has the relation of Eq. (9).

III. Discretizing into Finite Elements

Here, the conductor is discretized into triangular finite elements and the current function V is represented by the linear function of nodal values of current function for simplicity. It is easy to formulate the discretization by finite elements with more general shapes and functions of higher order. The value of the current function at each node is denoted by a nodal value of current function V_n ($n = 1,..., N_{\text{node}}$, N_{node} is the total number of nodes).

For each triangular element, there are three node numbers whose vertexes are i, j and k by numbering clockwise in the direction of normal unit vector $\mathbf{n}$; any position in the element is represented by the local coordinates L_i, L_j and L_k as

$$\mathbf{x} = L_i\mathbf{x}_i + L_j\mathbf{x}_j + L_k\mathbf{x}_k, \tag{12}$$

here $\mathbf{x}_i$, $\mathbf{x}_j$ and $\mathbf{x}_k$ are positions of vertexes and

$$L_i + L_j + L_k = 1 \qquad \text{and} \qquad 0 \leqslant L_i, L_j, L_k \leqslant 1. \tag{13}$$

The local coordinate L_i is given by

$$L_i = \frac{\Delta_{pjk}}{\Delta_e}, \tag{14}$$

here Δ_e and Δ_{pjk} are areas of the element and the triangular p–j–k, respectively, as shown in Fig. 3. The current function at the point $\mathbf{x}$ given by Eq. (12) is given by nodal values of current function V_i, V_j and V_k as

$$V = L_i V_i + L_j V_j + L_k V_k . \tag{15}$$

The current density is given by substituting Eq. (15) into Eq. (1) as

$$\mathbf{j} = V_i \mathbf{e}_i + V_j \mathbf{e}_j + V_k \mathbf{e}_k , \tag{16}$$

here

$$\mathbf{e}_i = \frac{\mathbf{x}_k - \mathbf{x}_j}{2\Delta_e}, \qquad \mathbf{e}_j = \frac{\mathbf{x}_i - \mathbf{x}_k}{2\Delta_e}, \qquad \mathbf{e}_k = \frac{\mathbf{x}_j - \mathbf{x}_i}{2\Delta_e} . \tag{17}$$

By substituting Eq. (16) into Eq. (3) the total magnetic energy is given by

$$U_m = \tfrac{1}{2} \sum_{i=1}^{N_{\text{node}}} \sum_{i'=1}^{N_{\text{node}}} M_{ii'} V_i V_{i'} , \tag{18}$$

here

$$M_{ii'} = \frac{\mu_0}{4\pi} \sum_e \sum_{e'} \int_e \int_{e'} \frac{\mathbf{e}_i \cdot \mathbf{e}_{i'}}{|\mathbf{x} - \mathbf{x}'|} \, ds \, ds', \tag{19}$$

and in Eq. (19), the double area integrations are summed for the elements e one node number whose vertexes are i and the elements e' one node number whose vertexes are i'. By substituting Eq. (16) into Eq. (5), the total Joule loss per unit time is given by

$$W_j = \sum_{i=1}^{N_{\text{node}}} \sum_{i'=1}^{N_{\text{node}}} R_{ii'} V_i V_{i'} , \tag{20}$$

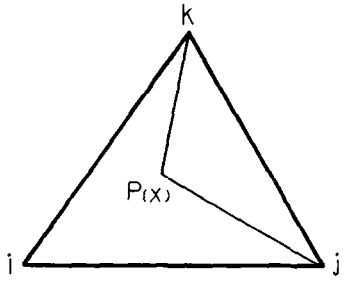

FIG. 3. A triangular finite element.

here

$$R_{ii'} = \sum_e \int_e (e_{\|i} e_{\|i'} \rho_{\|} + e_{\_i} e_{\_i'} \rho_{\_}) \, ds \tag{21}$$

and $e_{\|i} = \mathbf{e}_i \cdot \boldsymbol{\tau}_{\|}$ and $e_{\_i} = \mathbf{e}_i \cdot \boldsymbol{\tau}_{\_}$. In Eq. (21), the integrations are summed for the elements e, two node numbers whose vertexes are i and i'. By substituting Eq. (16) into Eq. (4), the mutual magnetic energy is given by

$$U_e = \sum_{i=1}^{N_{\text{node}}} E_i V_i \,. \tag{22}$$

here

$$E_i = \sum_e \int_e \mathbf{A}^{\text{ex}} \cdot \mathbf{e}_i \, ds, \tag{23}$$

and in Eq. (23), the integrations are summed for the elements e, one node number whose vertexes are i.

The matrices $\mathbf{M}$ and $\mathbf{R}$ whose components are $M_{ii'}$ and $R_{ii'}$ $(i, i' = 1,..., N_{\text{node}})$ are called inductance and resistance matrices, respectively, and symmetric and positive-definite matrices because of the physical meaning. And $\mathbf{E}$ whose components are E_i are called the externally applied voltage. When the conductor is symmetric for a certain transformation, if the points i and i' are transformed to the points j and j', respectively,

$$M_{jj'} = M_{ii'}, \qquad R_{jj'} = R_{ii'}, \qquad E_j = E_i \,. \tag{24}$$

The boundary conditions, symmetry conditions and the condition that the current function at a certain point of each subconductor is equal to zero are represented by the relation given by

$$\mathbf{V} = \mathbf{H}\,\mathbf{V}^0, \tag{25}$$

where $\mathbf{V}$ is a vector whose components are the nodal values of current function, $\mathbf{V}^0$ is a vector whose components are independent variables and whose dimension, N_{ind}, is equal to N_{node} minus the total number of independent conditions. The matrix $\mathbf{H}$ is a $N_{\text{node}} \times N_{\text{ind}}$ matrix.

By substituting Eq. (25) into Eqs. (18), (20) and (22), the summations are represented by independent variables as

$$U_m = \tfrac{1}{2}\mathbf{V}^t \mathbf{M}\,\mathbf{V} = \tfrac{1}{2}\mathbf{V}^{0t}\mathbf{M}^0\,\mathbf{V}^0$$

$$W_j = \mathbf{V}^t \mathbf{R}\,\mathbf{V} = \mathbf{V}^{0t}\mathbf{R}^0\,\mathbf{V}^0$$

and

$$U_e = \mathbf{E}^t\,\mathbf{V} = \mathbf{E}^{0t}\,\mathbf{V}^0, \tag{26}$$

where

$$\mathbf{M}^0 = \mathbf{H}^t \mathbf{M}\, \mathbf{H}, \qquad \mathbf{R}^0 = \mathbf{H}^t \mathbf{R}\, \mathbf{H}, \qquad \mathbf{E}^0 = \mathbf{H}^t \mathbf{E}. \tag{27}$$

The superscript t denotes the transposition of the matrices. The reduced matrices $\mathbf{M}^0$ and $\mathbf{R}^0$ are also symmetric and positive-definite matrices.

The "Lagrangian" of the system is $\mathscr{L} = U_m + U_e$ and the "dissipative function" is $\mathscr{R} = W_{j/2}$. "Lagrangian's equation" is [7],

$$\frac{d}{dt}\frac{\partial \mathscr{L}}{\partial \mathbf{V}^0} = -\frac{\partial \mathscr{R}}{\partial \mathbf{V}^0}. \tag{28}$$

Here the term of the electric field energy is neglected. Equation (28) is reduced into the circuit equation of the independent variables as,

$$\mathbf{M}^0 \frac{d\mathbf{V}^0}{dt} + \mathbf{R}^0\, \mathbf{V}^0 = -\frac{d\mathbf{E}^0}{dt}. \tag{29}$$

This equation is a N_{ind}-dimensional first order differential equation, and can be solved numerically using the Runge–Kutta method or the method of the expansion by eigenvectors [1].

IV. Applications

IV.1. *A Sphere Surface*

The eddy current on a sphere surface with a uniform area resistivity is formulated in Appendix A. Here consider a sphere surface of radius $a = 1$ m and electric area resistivity $\rho = 1\ \Omega$ and suppose that the current function V is symmetric to $\phi = 0$ and $\phi = \pi/2$ and antisymmetric to $\theta = \pi/2$. In this case, the terms of Eq. (A.4) are summed for odd numbers n's and even numbers m's.

In the numerical calculation, the sphere surface is discretized as shown in Fig. 4 in four different cases a, b, c and d. In Fig. 4, a part ($0 \leqslant \phi \leqslant \pi/2$, $0 \leqslant \theta \leqslant \pi/2$) is projected to the $z = 0$ plane. The numbers of elements N_e's are 25, 100, 225 and 100 in cases a, b, c and d, respectively. The discretizations are symmetric to $\phi = \pi/4$ in cases a, b and c and asymmetric in case d.

The eigenvalues (Eq. (A.7)) and the relative errors are shown in Table I for the formula and the numerical solutions. The current functions of eigenmodes (Eq. (A.5)) are also numerically calculated and the errors show the same tendency as those of the eigenvalues. It is evident from Table I that more accurate eigenvalues are calculated for finer meshes and lower mode numbers. It shows that the dimensions of elements must be small enough compared with the characteristic length of current distribution for accurate calculations.

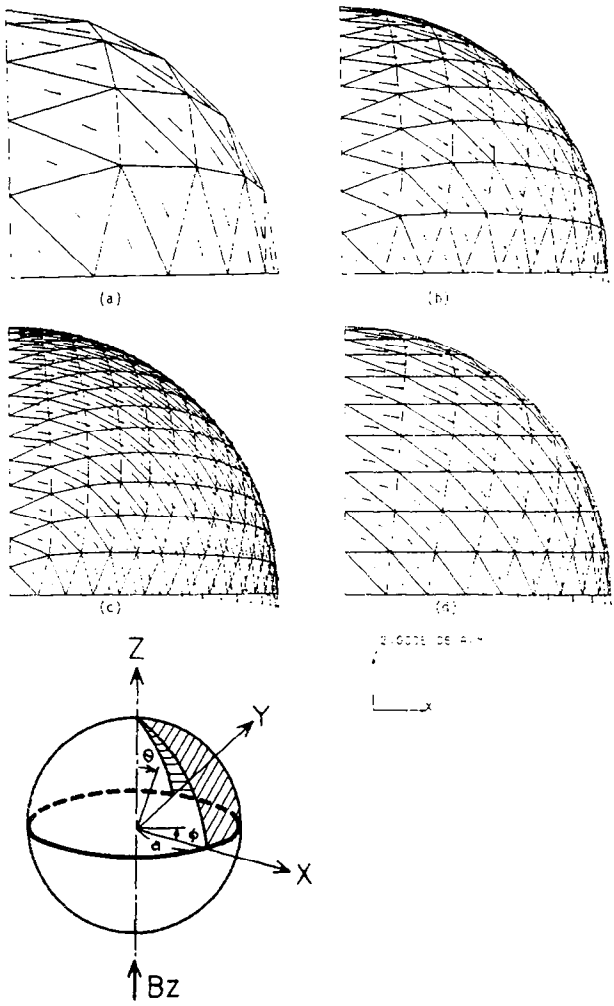

FIG. 4. Finite elements and current distributions on a sphere. (a) $N_e = 25$, (b) $N_e = 100$, (c) $N_e = 225$ and (d) $N_e = 100$.

We consider the case where a uniform magnetic field $B_z = 1$ T in the z direction is exerted suddenly at $t = 0$ on the sphere surface. The current distributions at $t = 10^{-7}$ sec are shown in Fig. 4 and the current functions at $t = 10^{-7}$ sec on the x axis and the variations of the Joule losses all over the sphere surface are shown with the relative errors in Tables II and III, respectively. In this case, only the (1, 0) mode is induced, so the errors show the same tendency as the errors of the eigenvalues of the (1, 0) mode. There is no significant difference between cases b and d.

It is evident that the results by this method correspond well to the analytic results and are more accurate as the meshes are finer.

TABLE I

Eigenvalues ($\times 10^{-7}$ sec) of Eigenmodes on a Sphere ($a = 1$ m, $\rho = 1\ \Omega$) and Relative Errors (%)

Mode No. (n, m)	Formula	Case a ($N_e = 25$)	Case b ($N_e = 100$)	Case c ($N_e = 225$)	Case d ($N_e = 100$)
(1, 0)	4.1888	4.1000	4.1785	4.1835	4.1811
		2.12	0.25	0.13	0.18
(3, 0)	1.7952	1.6239	1.7557	1.7771	1.7554
		9.54	2.20	1.01	2.22
(3, 2)	1.7952	1.6288	1.7544	1.7768	1.7496
		9.27	2.27	1.02	2.54
(5, 0)	1.1424	0.9652	1.0847	1.1161	1.0815
		15.51	5.05	2.30	5.33
(5, 2)	1.1424	0.9404	1.0759	1.1120	1.0713
		17.68	5.82	2.66	6.22
(5, 4)	1.1424	0.8831	1.0759	1.1034	1.0560
		22.70	5.82	3.41	7.56

IV.2. *A Square Plate*

When a uniform magnetic field with constant rate of change is exerted normally to a rectangular plate, the current function is given by [8],

$$V(x, y) = \frac{1}{2}\frac{\dot{B}}{\rho}\left\{x^2 - a^2 + \frac{32a^2}{\pi^3}\sum_{n=0}^{\infty}\frac{(-1)^n}{(2n+1)^3\cosh(2n+1)(\pi b/2a)} \times \cosh(2n+1)\frac{\pi y}{2a}\cdot\cos(2n+1)\frac{\pi x}{2a}\right\}, \tag{30}$$

TABLE II

Current Function $V(\theta, \phi = 0)$ ($\times 10^5$ A/m) and Relative Errors (%) at $t = 10^{-7}$ sec.

θ (degree)	Formula	Case a ($N_e = 25$)	Case b ($N_e = 100$)	Case c ($N_e = 225$)	Case d ($N_e = 100$)
0	9.402	9.155	9.308	9.358	9.298
		2.63	1.00	0.47	1.11
18	8.941	8.842	8.903	8.926	8.894
		1.11	0.43	0.17	0.53
36	7.606	7.553	7.576	7.593	7.567
		0.70	0.39	0.17	0.51
54	5.526	5.478	5.502	5.516	5.497
		0.87	0.43	0.18	0.52
72	2.905	2.869	2.891	2.899	2.888
		1.24	0.48	0.21	0.59

TABLE III

Joule Loss ($\times 10^{14}$ W) and Relative Errors (%)

Time ($\times 10^{-7}$)	Formula	Case a ($N_e = 25$)	Case b ($N_e = 100$)	Case c ($N_e = 225$)	Case d ($N_e = 100$)
1	7.4049	7.0377	7.2799	7.3501	7.2664
		4.96	1.69	0.74	1.87
2	4.5937	4.3209	4.5108	4.5569	4.5038
		5.94	1.80	0.80	1.96
3	2.8497	2.6529	2.7950	2.8252	2.7915
		6.91	1.92	0.86	2.04
4	1.7678	1.6288	1.7318	1.7516	1.7302
		7.86	2.04	0.92	2.13
5	1.0967	1.0005	1.0731	1.0859	1.0724
		8.36	2.15	0.98	2.22
6	0.6803	0.6140	0.6649	0.6733	0.6647
		9.75	2.26	1.03	2.29
7	0.4220	0.3770	0.4120	0.4174	0.4120
		10.66	2.37	1.09	2.37
8	0.2618	0.2315	0.2553	0.2588	0.2553
		11.57	2.48	1.15	2.48
9	0.1624	0.1421	0.1582	0.1604	0.1583
		12.50	2.59	1.23	2.52
10	0.1008	0.0873	0.0980	0.0995	0.0981
		13.39	2.78	1.29	2.68

here $2a$, $2b$ and ρ are the x dimension, the y dimension and the electric area resistivity of the plate and $\dot{B}$ is the rate of the change of the external magnetic field. On the boundary, $V = 0$.

Now we consider a case where $a = 1$ m, $b = 1$ m, $\rho = 1\ \Omega$ and $\dot{B} = 1$ T/sec. In the numerical calculation, the square plate is discretized as shown in Fig. 5 in the different cases a, b and c. In Fig. 5, a part ($0 \leqslant y \leqslant x$) is shown. The current function is symmetric to $y = 0$ and to the rotation of $\pi/2$ around the z axis. The numbers of elements are 25, 100 and 91 in cases a, b and c, respectively. In case c, the region near the boundary is divided into smaller elements because of the higher current density.

The current distributions which are time independent are shown in Fig. 5. In Table IV, the current functions on the x axis and the errors are shown for Eq. (30) and the numerical solutions. In case c, the fine distribution near the boundary can be seen and the errors are smaller near the boundary than the errors in cases a and b.

It is shown here that there is no problem in using elements of different dimensions at the same time in our method and it is effective to divide into smaller elements at the region where the current density is higher or the detail distribution must be calculated.

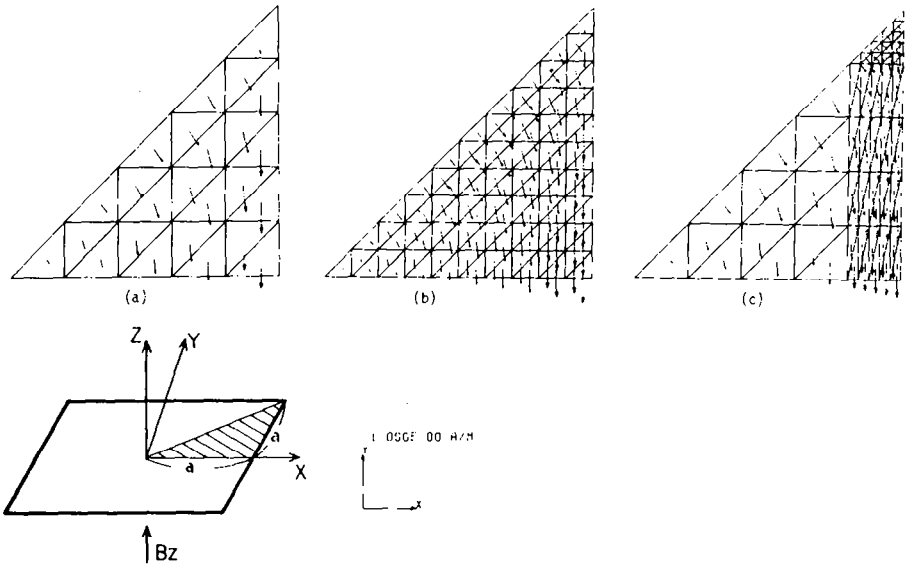

FIG. 5. Finite elements and current distributions on a square plate. (a) $N_e = 25$, (b) $N_e = 100$ and (c) $N_e = 81$.

TABLE IV

Current Function $V(x, y = 0)$ (A) and Relative Errors (%) on a Square Plate ($a = 1$ m, $b = 1$ m and $\rho = 1\ \Omega$)

x (m)	Formula	Case a ($N_e = 25$)	Case b ($N_e = 100$)	Case c ($N_e = 81$)
0.0	0.2946	0.2994	0.2963	0.3000
		1.63	0.58	1.84
0.2	0.2846	0.2861	0.2850	0.2866
		0.52	0.14	0.70
0.4	0.2535	0.2537	0.2536	0.2542
		0.07	0.03	0.27
0.6	0.1988	0.1985	0.1988	0.1987
		0.15	0.01	0.05
0.8	0.1162	0.1159	0.1161	0.1150
		0.23	0.06	1.01
0.84	0.09582	0.09272	0.09472	0.09499
		3.23	1.15	0.86
0.88	0.07408	0.06954	0.07333	0.07351
		6.12	1.01	0.77
0.92	0.05090	0.04636	0.05011	0.05055
		8.91	1.54	0.68
0.96	0.02622	0.02318	0.02506	0.02605
		11.60	4.43	0.65

IV.3. *INTOR-J Primary Shield*

We analyze the eddy current on the primary shield of INTOR-J design [9] when the plasma current disrupts rapidly. The calculational model is shown in Fig. 6. Half of one sector of the primary shield is composed of an inner plate, an outer plate and two side plates. The plates are welded and conduct mutually. The sectors are connected by bellows and form a torus. Actually there is a plate at the toroidal angle $\phi = 0$ but it is negligible because there is no current on it because of the symmetry. The current function is symmetric to the $y = 0$ plane and the rotation of 30° around the z axis and antisymmetric to the $z = 0$ plane.

The material of the plates and bellows is stainless steel and electric volume resistivity ρ is 7.2×10^{-8} Ωm. The outer plate, the inner plate, side plate 1 and side plate 2 are 4, 12, 3 and 10 cm in thickness, respectively. The bellows is supposed to have effective area resistivities in the toroidal and poloidal directions given by

$$\rho_t^{\text{eff}} = \frac{\rho f}{d} \qquad \text{and} \qquad \rho_p^{\text{eff}} = \frac{\rho}{df}, \tag{31}$$

here $d = 1.5$ mm and $f = 8.2/R$ (m). R is the distance from the z axis. The 12 bellows have the total one-turn resistance 0.2 mΩ in the toroidal direction.

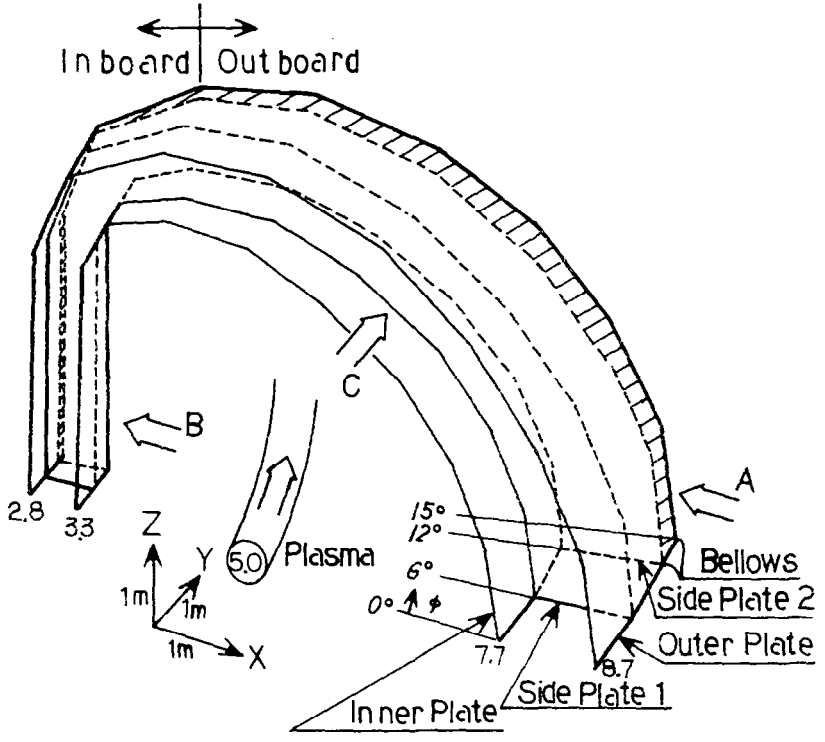

FIG. 6. A calculational model of INTOR-J primary shield.

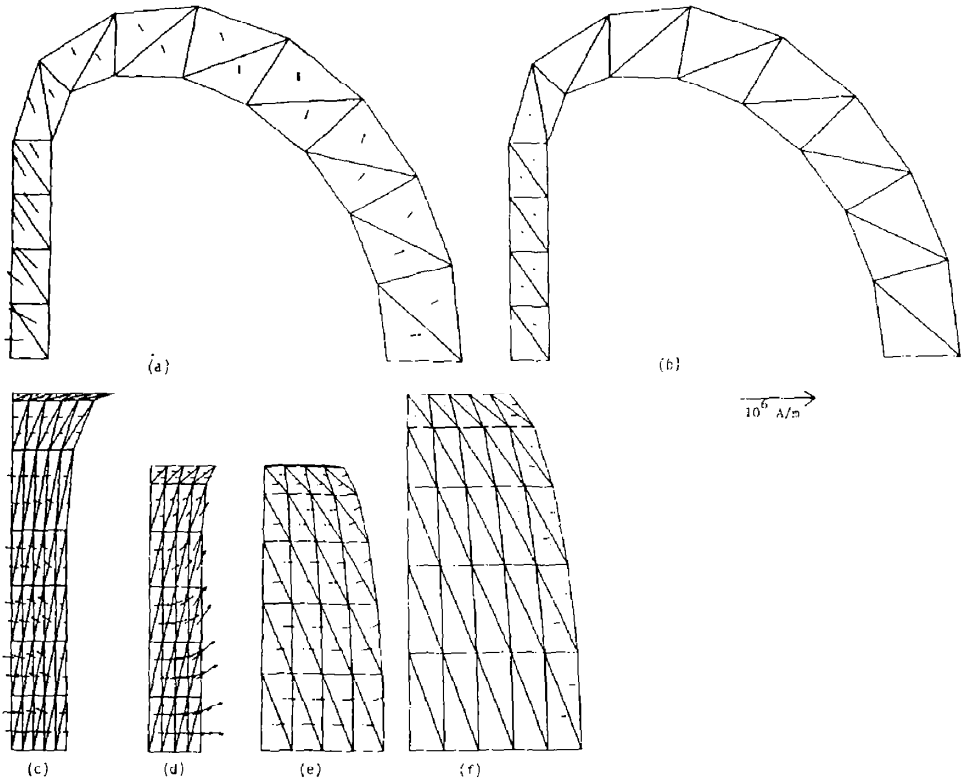

FIG. 7. Eddy current distributions on INTOR-J primary shield. (a) Side plate 2 viewed toward *C*. (b) Side plate 1 viewed toward *C*. (c) Inboard of outer plate viewed toward *B*. (d) Inboard of inner plate viewed toward *B*. (e) Outboard of inner plate viewed toward *A*. (f) Outboard of outer plate viewed toward *A*.

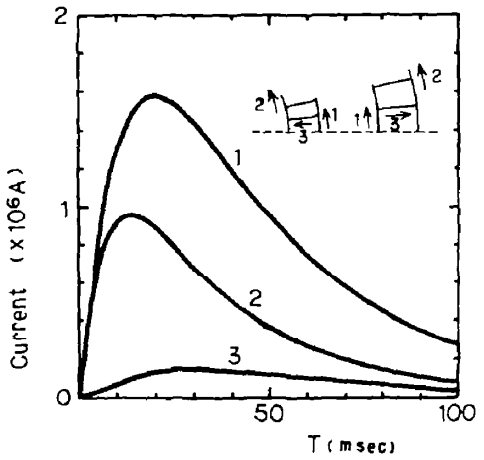

FIG. 8. Variations of integrated currents flowing through plates.

The plasma current is supposed to decay as

$$I_p = I_{p0}\, e^{-t/\tau} \qquad (I_{p0} = 4.7 \text{ MA}, \tau = 10 \text{ msec}) \tag{32}$$

and is approximated by a ring current of the major radius of 5.0 m.

The current distribution at 20 msec after the initiation of the plasma current decay is shown in Fig. 7. The current flows in the direction of the plasma current at the inner plate and into the outer plate and the bellows through side plate 2. The currents in side plate 1 and the outboard of the outer plate are low. The toroidal current distribution is flat in the poloidal direction at the bellows.

In Fig. 8, the variations of the integrated currents through plates in the toroidal direction are shown. The integrations are over the upper half in the poloidal direction. The one-turn current through the bellows shown by line 2 has the maximum value 0.96 MA at 15 msec and the current through the outer plate shown by line 1 minus line 2 has the maximum value 0.76 MA at 30 msec.

V. Conclusions

In our numerical method, the thin conductors are discretized to finite elements and lumped electric constants (inductances, resistances and applied voltages) are integrated for the distributed currents on the elements. The circuit equations are solved in the usual manner of the inductance and resistance circuits.

Because the conductors are discretized in the same manner of the finite elements method, the method has the following advantages:

(a) The non-uniform and non-isotropic electric resistivities are treated.

(b) It is easy to discretize arbitrarily shaped conductors into finite elements and to discretize a certain region into finer elements.

(c) The boundary and symmetry conditions are easily included.

The method is also applicable to arbitrarily connected conductors by means of the boundary conditions which have the same meaning of Kirchhoff's first law.

The resistance and inductance matrices are symmetric and positive-definite, so it is a mathematically trivial problem to solve the circuit equations. The numerically calculated eigenmodes and eigenvalues correspond to the independent current modes and their time constants in physical meaning as shown in the application to a sphere surface. So it is possible to investigate the response of the eddy current qualitatively or quantitatively by means of the calculated eigenmodes and eigenvalues.

In the applications to a sphere surface and a square plate, it is shown that the numerical results correspond well to the results given by the formulas and the accuracy is raised by finer elements. It is also shown that it is efficient to discretize certain regions into finer elements. In the application to the INTOR-J primary shield, it is shown that this method is applicable and efficient for the eddy current calculations of thin complicated conductors with arbitrary connections and shapes.

APPNDIX A: EDDY CURRENTS ON A SPHERE SURFACE

It is possible to formulate analytically the eddy currents on a sphere surface with a uniform resistivity by the expansion of spherical harmonic functions. We consider a sphere surface with the radius a and the area resistivity ρ and let (r, θ, ϕ) to be the spherical coordinate.

Any external magnetic field can be represented by a magnetic scalar potential as

$$\mathbf{B}^{ex} = -\nabla \Psi^{ex}, \tag{A.1}$$

and the magnetic scalar potential symmetric to $\phi = 0$ can be expanded by the spherical harmonic functions as

$$\Psi^{ex} = \sum_{n=1}^{\infty} \sum_{m=0}^{n} e_n^m \Psi_n^m, \tag{A.2}$$

here

$$\Psi_n^0 = \frac{\mu_0}{2} \sqrt{\frac{a(n+1)}{\pi n(2n+1)}} \left(\frac{r}{a}\right)^n P_n(\cos\theta)$$

and

$$\Psi_n^m = \mu_0 \sqrt{\frac{a(n-m)!(n+1)}{2\pi(n+m)!\, n(2n+1)}} \left(\frac{r}{a}\right)^n P_n^m(\cos\theta) \cos m\phi \qquad (\text{for } m \neq 0). \tag{A.3}$$

P_n's and P_n^m's are Legendre's functions and associated Legendre's functions. The coefficients e_n^m's are functions of time.

When the external magnetic field given by Eq. (A.2), is exerted, the current function of the induced eddy current is given by

$$V = \sum_{n=1}^{\infty} \sum_{m=0}^{n} a_n^m Y_n^m, \tag{A.4}$$

here

$$Y_n^0 = \frac{1}{2} \sqrt{\frac{a(2n+1)}{\pi n(n+1)}} P_n(\cos\theta)$$

and

$$Y_n^m = \sqrt{\frac{a(n-m)!\,(2n+1)}{2\pi(n+m)!\, n(n+1)}} P_n^m(\cos\theta) \cos m\phi \qquad (\text{for } m \neq 0). \tag{A.5}$$

The independent equations of the coefficients a_n^m's are given by

$$\frac{d}{dt} a_n^m + \frac{1}{\tau_n^m} a_n^m = -\frac{d}{dt} e_n^m, \tag{A.6}$$

here

$$\tau_n^m = \frac{\mu_0 a}{\rho(2n+1)}. \tag{A.7}$$

The functions Y_n^m's represent eigenmodes of the current on a sphere and τ_n^m's represent their eigenvalues. The components of the current density are given by

$$j_\phi = -\frac{1}{a}\frac{\partial V}{\partial \theta} \quad \text{and} \quad j_\theta = \frac{1}{a\sin\theta}\frac{\partial V}{\partial \phi}. \tag{A.8}$$

When a uniform magnetic field in the z direction B_z is exerted on the sphere surface, the magnetic scalar potential is given by

$$\Psi^{ex} = -B_z \cdot z = -B_z\, r\, P(\cos\theta) = e_1^1\, \Psi_1^1, \tag{A.9}$$

here

$$e_1^1 = -\frac{\sqrt{6\pi a}}{\mu_0} B_z. \tag{A.10}$$

If we represent the current density as

$$j_\phi = j^0 \cos\theta \quad \text{and} \quad j_\theta = 0, \tag{A.11}$$

for j^0,

$$\frac{dj^0}{dt} + \frac{j^0}{\tau_1^1} = -\frac{3}{2\mu_0}\frac{d}{dt}B_z, \tag{A.12}$$

here

$$\tau_1^1 = \frac{\mu_0 a}{3\rho}. \tag{A.13}$$

ACKNOWLEDGMENTS

The author is indebted to Dr. S. Shimamoto and Mr. K. Oka of the Japan Atomic Energy Research Institute for their support of this work and for the permission to publish this paper. The author also wishes to thank Mr. N. Asami, Dr. M. Nishikawa and Mr. M. Yamada of Mitsubishi Atomic Power Industries, Inc. for their constant encouragement.

REFERENCES

1. A. KAMEARI AND Y. SUZUKI, *in* "Proceedings, 7th Symposium on Engineering Problems of Fusion Research, 1977," p. 1385.
2. H. T. YEH, *in* "Proceedings 7th Symposium on Engineering Problems of Fusion Research, 1977," p. 1318.
3. T. KOBAYASHI, *Japan J. Appl. Phys.* **18** (1979), 2003.
4. U. R. CHRISTENSEN, Princeton Plasma Physics Laboratory-1516, 1979.
5. T. TAKAHASHI, G. TAKAHASHI, Y. KAZAWA, AND Y. SUZUKI, *in* "Proceedings, 7th Symposium on Engineering Problems of Fusion Research, 1977," p. 1393.
6. L. A. TSEITLIN, *Sov. Phys. Tech. Phys.* **14** (1970), 1305.
7. L. D. LANDAU AND E. M. LIFSHITS, "Electrodynamics of Continuous Media," Section 48, Pergamon, Oxford/London/New York/Paris, 1960.
8. D. W. WEISSENBURGER AND U. R. CHRISTENSEN, Princeton Plasma Physics Laboratory-1517, 1979.
9. K. SAKO *et al.*, Japan Atomic Energy Research Institute-M 8518, 1979.